Time domain implementation of a spectral non-reflecting boundary condition for unsteady turbomachinery flows

Daniel Schlüß and Christian Frey
daniel.schluess@dlr.de
German Aerospace Center (DLR)
Institute of Propulsion Technology
51147 Cologne, Germany

ABSTRACT

We show the implementation of a spectral, non-reflecting boundary condition (NRBC) for time marching, unsteady simulations of flows in turbomachinery components. It is well known that reflections from artificial boundaries can impair the prediction of unsteady flow phenomena. In the context of turbomachinery flows, some frequency domain methods address this issue by means of spectral NRBC. Since these NRBC are non-local in space and time, their implementation in time domain solvers is not straightforward. We elaborate on these difficulties and on how we deal with them. Applications of the NRBC to a two-dimensional flutter configuration and to the prediction of rotor-stator interactions of a real fan configuration are shown. The most important feature of the presented method is the combination of increased robustness and good reflection properties.

Keywords: Non-reflecting boundary conditions; Unsteady flows; CFD methods; Aeroelasticity; Aeroacoustics

NOMENCLATURE

Latin symbols

a	Speed of sound
c	Chord length
h_t	Specific stagnation enthalpy
$\mathbf{i}$	Imaginary unit
k	Boundary-normal wave number
l	Circumferential wavenumber
L	Matrix of left eigenvectors to dispersion relation, Inverse of R
m	Non-dimensional circumferential wavenumber, equivalent to nodal diameter ($m = lr$)
m^*_{red}	Reduced mass flow normalised with nominal design conditions
Ma	Mach number
N	Number of time steps to resolve one fundamental period
p	Pressure
p_{dyn}	Dynamic pressure at entry (compressible definition)
r	Radius
R	Matrix of right eigenvectors to dispersion relation
$\mathrm{Re}\ q, \mathrm{Im}\ q$	Real and imaginery part of a complex quantity q
s	Specific entropy
t	Time
T	Period associated with fundamental frequency
U	Velocity magnitude
u, v, w	Velocity components along coordinates x, y and z
W_{cyc}	Aerodynamic work per cycle
x	Coordinate perpendicular to boundary or axial position
y	Circumferential coordinate ($y = r\vartheta$)
z	Coordinate tangent to boundary, but perpendicular to y

Greek symbols

$\alpha_{rad}, \alpha_{circ}$	Radial and circumferential flow angles
γ	Heat capacity ratio
Π^*	Stagnation pressure ratio normalised with nominal design conditions
ρ	Density
σ	Inter-blade phase angle (IBPA)
Ξ	Non-dimensional aerodynamic damping coefficient
ω	Angular frequency

Subscripts and superscripts

q_f	State at a boundary face
R_{1D}, L_{1D}	One-dimensional eigenvector matrices
$\hat{q}$	Fourier coefficient of q
$\overline{q}$	Temporal and area average of q
$\widetilde{q}$	Instantaneous area average of q
q^F	Flux or mixed-out average of q
q'	Disturbance in q from $\overline{q}$
$x^{in,out}$	Incoming and outgoing components of vectors or associated rows and columns of matrices x

Abbreviations

BPF	Blade passing frequency
CFD	Computational Fluid Dynamics
DFT	Discrete Fourier transform
IBPA	Inter-blade phase angle
NRBC	Non-reflecting boundary conditions
(U)RANS	(Unsteady) Reynolds-averaged Navier-Stokes
VPF	Vane passing frequency

1.0 INTRODUCTION

To further improve aircraft engines with respect to efficiency and weight, the design of turbomachinery components tends to aerodynamically and mechanically highly loaded blades with relatively small axial spacing and low structural damping. With this, the demand to capture the associated, unsteady flow phenomena drastically increases. Aerodynamic evaluation of blade row interaction as well as aeroelasticic and aeroacoustic analysis rely on a highly accurate prediction of unsteady flows.

Due to ongoing progress in the development of hardware resources and software tools, URANS simulations have become affordable and suffiently fast not only for academic purposes but also for everyday industrial design. However, numerical reflections arising from artificial, open boundaries at finite computational domains can strongly deteriorate the flow solution and especially the accurate prediction of unsteady pressure fluctuations.

For turbomachinery flows, which are dominated by periodically unsteady effects, linear and non-linear frequency domain methods have emerged as highly efficient means (see e.g. [1, 2, 3, 4]). These approaches solve the Fourier-transformed URANS equations for distinct frequencies of interest, usually blade interaction frequencies or frequencies of the structural eigenmodes of the blades and possibly higher harmonics. Another advantage of frequency domain methods is that, in the frequency domain, the boundary flow field can be decomposed into waves with known direction of propagation. This allows for a non-reflecting boundary treatment in a relatively simple manner (cf. [5, 6, 7, 8]).

For time domain simulations, such boundary conditions are more complicated. However, there are several reasons why it seems desirable to conduct time domain simulations using this type of NRBC. Non-linear time domain simulations constitute the highest level of modeling unsteady flow phenomena in turbomachinery flows since frequency domain methods are only applicable if all fluctuations are strictly periodic and their frequencies are known. Therefore, phenomena like shock boundary layer interaction, unsteady wakes and vortex shedding pose challenges to frequency domain methods. Furthermore, robustness of these methods in combination with advanced turbulence and transition models is still a matter of research. Hence, even if efficient frequency domain methods are further improved and more and more employed in industrial design, time domain simulations remain important to generate valuable references for validating these methods in detail. For this reason, we consider it a benefit to have identical spectral boundary conditions available for time and frequency domain simulations.

There are different types of unsteady boundary conditions. Simple boundary conditions based upon one-dimensional characteristics offer insufficient reflection properties for perturbations that do not impinge perpendicularly on the boundary surface. Giles describes the concept of modal decomposition for NRBC, but proposes to circumvent the calculation of Fourier coefficients [9]. His approach is to develop a second order Taylor series expansion of the underlying eigenvalue problem yielding a PDE that can be solved in time domain. This method is rather popular, but proves to be of limited accuracy when the flow conditions strongly deviate from the assumptions made for the series expansion [10, 11]. A time-local, but spatially non-local extension to higher order by Goodrich and Hagstrom [12] shows better reflection properties, but it is restricted to circumferentially periodic flows. Thus, this method can neither be used for single passage simulations of arbitrary blade row interactions nor for flutter simulations with arbitrary IBPA. Chassaing and

Gerolymos present a time domain implementation of exact spectral NRBCs with good reflection properties [10]. Yet, they observe slow convergence for a rather simple test case. Their investigation considers plane acoustic waves imposed on a subsonic, homogeneous background flow. The authors of the present paper have made similar experiences with a former ad-hoc adoption of spectral boundary conditions from their harmonic balance solver (cf. [13]) using the Fourier coefficients provided by the phase lag algorithm [11]. This implementation seemed promising in terms of its reflection properties, but lacked robustness for many configurations beyond basic test cases.

Therefore, we present a reworked implementation of spectral NRBC for dual time-stepping time domain simulations in this paper. Time domain specific aspects are addressed. We put special emphasis on how to calculate temporally non-local Fourier coefficients, the distinction, which steps of the boundary treatment take place in physical time and which ones in pseudo-time, and how we significantly improved the stability in our implementation.

We present two relevant turbomachinery test cases in order to show the good robustness and convergence characteristics as well as reflection properties of our implementation. Firstly, we study the two-dimensional flutter test case standard configuration ten [14], which is known to be sensitive to reflections from artificial boundaries. DLR's ultra high bypass ratio fan (UHBR) will serve to verify the applicabilty of our implementation to realistic turbomachinery configurations.

2.0 SPECTRAL NRBC FOR TIME DOMAIN SOLVERS

2.1 Theory

The concept of the NRBC presented in this paper is to consider the boundary flow field in the spectral domain, i.e. in the wavenumber and frequency domain. Here, the flow can be decomposed into waves with known propagation properties. To attain non-reflecting behaviour of artificial open boundaries, incoming waves can easily be suppressed by setting their amplitude to zero and reconstructing the flow in the physical domain, i.e. in time and space, allowing only outward travelling disturbances from the mean flow.

For this purpose, we assume the flow at the boundaries is dominated by two-dimensional effects in blade-to-blade stream surfaces disregarding disturbances in radial direction. In this work, the surface is defined by the boundary-normal and the pitchwise direction. We further assume the boundary flow is approximately inviscid and all disturbances from an underlying mean flow are sufficiently small. Therefore, we derive the NRBC from the linearised quasi-two-dimensional Euler equations

$$\frac{\partial q'}{\partial t} + A\frac{\partial q'}{\partial x} + B\frac{\partial q'}{\partial y} = 0 \tag{1}$$

with

$$A = \begin{pmatrix} \overline{u} & \overline{\varrho} & 0 & 0 & 0 \\ 0 & \overline{u} & 0 & 0 & 1/\overline{\varrho} \\ 0 & 0 & \overline{u} & 0 & 0 \\ 0 & 0 & 0 & \overline{u} & 0 \\ 0 & \gamma\overline{p} & 0 & 0 & \overline{u} \end{pmatrix}, \quad B = \begin{pmatrix} \overline{v} & 0 & \overline{\varrho} & 0 & 0 \\ 0 & \overline{v} & 0 & 0 & 0 \\ 0 & 0 & \overline{v} & 0 & 1/\overline{\varrho} \\ 0 & 0 & 0 & \overline{v} & 0 \\ 0 & 0 & \gamma\overline{p} & 0 & \overline{v} \end{pmatrix}, \quad q = \begin{pmatrix} \rho \\ u \\ v \\ w \\ p \end{pmatrix}. \tag{2}$$

Here x is alinged with the boundary normal in mean flow direction (i.e. inward pointing at an inflow boundary and vice versa) and $y = r\vartheta$ denotes the pitchwise direction, each with corresponding velocity components u and v. The third velocity component w is tangent to the boundary and prependicular to the aforementioned directions, such that it is exactly radial if the boundary is not inclined

but at constant axial position. Note that, at any radial position of a boundary, the flow state $q(y,t)$ is the sum of a temporal and circumferential area average $\overline{q}$ and a fluctuation $q'(y,t)$.

In the context of the linearised Euler equations, we may describe an arbitrary flow field by superposition of wave-like solutions of the following form:

$$q' = \mathrm{Re}\left(\hat{q}\, e^{\mathrm{i}(kx+ly+\omega t)}\right) \tag{3}$$

For non-zero amplitudes $\hat{q}$, Eqn. (1) is simplified to the dispersion relation:

$$\det\left(\omega I + kA + lB\right) = 0 \tag{4}$$

or equivalently

$$\det\left(\omega A^{-1} + kI + lA^{-1}B\right) = 0. \tag{5}$$

Since this equation describes the relation of the wavenumber components and the angular frequency, it is helpful for the distinction of upstream and downstream propagating waves. If we now conduct a Fourier transform of the boundary flow field in time as well as in circumferential direction, then we can rewrite Eqn. (5) as an eigenvalue problem with eigenvalues $-k_i$ and eigenvectors r_i for any known circumferential wavenumber l and angular frequency ω:

$$\left(\omega A^{-1} + lA^{-1}B\right) r_i = -k r_i. \tag{6}$$

As for three-dimensional flows Eqn. (5) is a five-dimensional system, there are five eigenvalues with corresponding eigenvectors. A possible set of eigenvectors reads as follows:

$$r_1 = \begin{pmatrix} -\overline{\varrho} \\ 0 \\ 0 \\ 0 \\ 0 \end{pmatrix}, \quad r_2 = \begin{pmatrix} 0 \\ \overline{a}lr \\ \frac{\overline{a}}{\overline{u}}\left(\omega r + lrv\right) \\ 0 \\ 0 \end{pmatrix}, \quad r_3 = \begin{pmatrix} 0 \\ 0 \\ 0 \\ \overline{a} \\ 0 \end{pmatrix} \quad r_{4,5} = \begin{pmatrix} \overline{\varrho} \\ \frac{-\overline{a}^2 k_{4,5}}{k_{4,5}\overline{u}+l\overline{v}+\omega} \\ \frac{-\overline{a}^2 l}{k_{4,5}\overline{u}+l\overline{v}+\omega} \\ 0 \\ \gamma p \end{pmatrix} \tag{7}$$

The first three eigenvectors are associated with a triple eigenvalue. While r_1 represents an entropy wave, r_2 and r_3 describe vorticity-like fluctuations in the underlying stream surface and out-of-plane fluctuations respectively. From their common eigenvalue we infer that these types of fluctuations propagate convectively.

The remaining eigenvectors $r_{4,5}$ represent acoustic, i.e. isentropic and irrotational, waves. The polynomial, from which the corresponding eigenvalues $k_{4,5}$ are determined, reduces to the quadratic equation $\left(\omega + k_{4,5}\overline{u} + l\overline{v}\right)^2 = \overline{a}^2\left(k_{4,5}^2 + l^2\right)$. As its roots may be real- or complex-valued, care must be taken in choosing the consistent side of the branch of the complex square root. In this work, we assume the flow is subsonic in the boundary-normal direction, which is true for most turbomachinery flows. Then, we can determine k_4 such that r_4 is a downstream propagating acoustic wave whereas r_5 propagates upstream. If $k_{4,5}$ are real, then Eqn. (3) reveals that the waves propagate with constant amplitude (cut on modes) whereas they decay if $k_{4,5}$ are complex-valued (cut off modes). For details and the explicit formulas of all eigenvalues and eigenvectors the reader may refer to [9, 5].

In case of acoustic resonance, i.e. at the transition from cut on to cut off acoustic modes, $k_{4,5}$ become equal, their right eigenvectors are linearly dependent and we are no longer able to find a basis of right eigenvectors. To avoid this, we add a small imaginary part to the otherwise real angular frequency. This can be interpreted as adding a little artificial damping to the wave-like solutions (3). A comprehensive discussion of this technique can be found in [15].

For the deduction of non-reflecting boundary conditions, we will use the fact that for any point in the spectral domain, the flow state $\hat{q}_{(\omega,l)}$ can be decomposed into a linear combination of the eigenvectors. The weights or amplitudes are obtained by means of the modal decomposition matrix L, i.e. the inverse of the right eigenvector matrix

$$L_{(\omega,l)} = R^{-1}_{(\omega,l)} = (r_1\ r_2\ r_3\ r_4\ r_5)^{-1}\,. \tag{8}$$

As the waves associated with the first four eigenvectors travel downstream, they enter the computational domain at an inflow boundary while the fifth wave is outgoing. At outflow boundaries, only the wave associated with the fifth eigenvector is incoming. To suppress reflections from an artificial boundary, we thus set the amplitude of any incoming wave to zero. This condition is given by

$$L^{in}_{(\omega,l)}\hat{q}_{(\omega,l)} = 0 \tag{9}$$

where L^{in} comprises the rows of L that correspond to incoming waves, viz. row one to four at inflow boundaries and row five at outlets.

2.2 Implementation in time domain solver

2.2.1 Calculation of Fourier coefficients

The approach from Section 2.1 requires the boundary flow field in its temporally and circumferentially Fourier-transformed representation as input quantities. Since frequency domain methods directly solve the Fourier-transformed URANS equations, they are non-local in time and provide the temporally transformed quantities naturally. For time marching simulations, we calculate the temporal Fourier coefficients in an iterative manner comparable to the harmonic store concept used for the phase lag technique (cf. [16, 17]). Instead of storing the boundary flow field history for the whole period of the fundamental frequency, we store temporal Fourier coefficients. We either store the full spectrum from the base frequency to the highest possible harmonics according to the Nyquist criterion or a predefined set of relevant harmonics if these can be estimated a priori. The Fourier coefficient of the k-th harmonic $\hat{q}_k$ of a fundamental angular frequency ω are updated at each physical time step n according to

$$\hat{q}^n_k = \hat{q}^{n-1}_k + \frac{1}{N}\left(q^n - {q_*}^n\right) e^{-\mathrm{i}k\omega t} \tag{10}$$

where N denotes the number of physical time steps per period of the fundamental frequency and ${q_*}^n$ is the current flow state as approximately reconstructed from the previous Fourier coefficients:

$$q_* = \sum_k \hat{q}^{n-1}_k e^{\mathrm{i}k\omega t} \tag{11}$$

To further conduct a circumferential Fourier transform of the temporal Fourier coefficients, we require the boundary to consist of bands of faces with their centres at constant radius. Then a DFT can be applied to each band.

2.2.2 Characteristics-based approach

In our understanding, several aspects greatly improve the robustness and convergence behaviour of the presented implementation as opposed to our former ad-hoc adoption from our harmonic balance solver (cf. [11, 5]).

Firstly, we use simple one-dimensional, characteristic boundary conditions as basic framework for these are well-posed (cf. [9]) and known to be very robust. For one-dimensional flows, i.e. if all waves enter or leave the domain perpendicularly to

the boundary, the circumferential wavenumber vanishes and the eigenvectors (cf. Eqn. (7)) can be scaled such that they do no longer depend on ω:

$$L_{1D} = \begin{pmatrix} \frac{-1}{\overline{\varrho}} & 0 & 0 & 0 & \frac{1}{\overline{\varrho}\,\overline{a}^2} \\ 0 & 0 & \frac{1}{\overline{a}} & 0 & 0 \\ 0 & 0 & 0 & \frac{1}{\overline{a}} & 0 \\ 0 & \frac{1}{a} & 0 & 0 & \frac{1}{\overline{\varrho}\,\overline{a}^2} \\ 0 & -\frac{1}{a} & 0 & 0 & \frac{1}{\overline{\varrho}\,\overline{a}^2} \end{pmatrix}, \quad R_{1D} = \begin{pmatrix} -\overline{\varrho} & 0 & 0 & \frac{\overline{\varrho}}{2} & \frac{\overline{\varrho}}{2} \\ 0 & 0 & 0 & \frac{\overline{a}}{2} & -\frac{\overline{a}}{2} \\ 0 & \overline{a} & 0 & 0 & 0 \\ 0 & 0 & \overline{a} & 0 & 0 \\ 0 & 0 & 0 & \frac{\overline{\varrho}\,\overline{a}^2}{2} & \frac{\overline{\varrho}\,\overline{a}^2}{2} \end{pmatrix}$$

The characteristic variables are then defined as $c = L_{1D}\ q'$. As they solely depend on mean flow quantities, the one-dimensional boundary condition

$$L_{1D}^{in}\ q' = 0 \tag{12}$$

can be applied locally. Further, we can construct the boundary state

$$q = \overline{q} + q' = \overline{q} + \left(R_{1D}^{in} c^{in} + R_{1D}^{out} c^{out}\right) \tag{13}$$

where the incoming characteristics need to be specified, viz. set to zero for one-dimensional NRBC, and the outgoing characteristics have to be extrapolated from the inner.

Instead of prescribing zero amplitude incoming characteristics (Eqn. (12)), we calculate local target values for incoming characteristics from the spectral two-dimensional NRBC theory. Analogously to Eqn. (13), we extrapolate Fourier-transformed characteristics in the spectral domain and reformulate Eqn. (9)

$$L_{(\omega,l)}^{in} \hat{q}_{(\omega,l)} = L^{in} \left(R_{1D}^{in}\ \hat{c}_{(\omega,l),target}^{in} + R_{1D}^{out}\ \hat{c}_{(\omega,l)}^{out}\right) = 0 \tag{14}$$

which can be solved for the incoming target characteristics $\hat{c}_{(\omega,l),target}^{in}$ yielding

$$\hat{c}_{target,(\omega,l)}^{in} = \left[- \left(L_{(\omega,l)}^{in} R_{1D}^{in}\right)^{-1} L_{(\omega,l)}^{in} R_{1D}^{out}\ \hat{c}_{(\omega,l)}^{out} \right]. \tag{15}$$

The instantaneous, face-wise target incoming characteristics need to be reconstructed by means of spatial and temporal inverse Fourier transforms. As the temporal Fourier coefficients of the boundary flow field are only updated once per physical time step, the local target characteristics also need to be calculated only once per time step. However, to ensure the target values are met at the end of a pseudo-time iteration loop, the local face characteristics must be updated at each pseudo-time step i:

$$c_{in,f}^{i} = (1 - \varphi)\ c_{in,f}^{i-1} + \varphi\ c_{in,target} \tag{16}$$

In our experience, a certain amount of relaxation is necessary to preserve the good robustness of the underlying characteristic boundary condition. On the other hand, the relaxation factor φ must be sufficiently large to achieve convergence in the pseudo-time within a limited number of iterations.

The mode $\hat{q}_{(0,0)}$ is not considered for determining the incoming target characteristics at each face since this mode describes the temporal and circumferential mean flow. Instead, we add the mean characteristic shift $\delta\overline{c^{in}}$ to the boundary state in order to meet user-specified boundary values, denoted by subscript *bd*. To specify $\delta\overline{c^{in}}$, we minimise the residuum

$$\mathfrak{R} = \begin{cases} \begin{pmatrix} \overline{p}(s^F - s_{bd}) \\ \overline{\varrho}\,\overline{a}\left(v^F - u^F \tan(\alpha_{circ,bd})\right) \\ \overline{\varrho}\,\overline{a}\left(w^F - u^F \tan(\alpha_{rad,bd})\right) \\ \overline{\varrho}(h_t^F - h_{t,bd}) \end{pmatrix} & \text{for inflow boundaries} \\ \\ \left(p^F - p_{bd}\right) & \text{for outflow boundaries} \end{cases} \tag{17}$$

by one Newton-Raphson step:

$$\mathfrak{R} + \frac{\partial \mathfrak{R}}{\partial q} R_{1D}^{in} \delta \overline{c^{in}} = 0 \tag{18}$$

Here, superscript F denotes temporally and spatially flux-averaged quantities (cf. [18, 19]). The resulting shift should be applied only once per physical time step for two reasons. Firstly, convergence of the inner iteration loop would otherwise be impossible because the time-mean boundary state cannot meet a given values in a single physical time step. Secondly, the (stability) properties of the dynamic system should not depend on the number of inner iterations per time step.

As the temporal development of time-mean quantities is lagged depending on the period over which the temporal averaging is defined, the dynamic properties, e.g. the stability limit for the control of boundary values, is also greatly affected by the underlying fundamental frequency. Therefore, the rate of change for the boundary flow must be chosen with respect to the number of time steps per period. To keep the convergence properties independent of the temporal resolution of a period, we suggest to scale $\delta \overline{c^{in}}$ by a factor $\frac{\psi \mathcal{N}}{N}$. The parameter ψ can be chosen in the range up to five in our experience. To accelerate multi-passage simulations, in which the dominant blade interaction frequencies are much greater than the underlying base frequency, e.g. the shaft revolution frequency in full wheel simulations, the number of considered passages in the neighbouring row $\mathcal{N}$ is also considered in the scaling factor. From the authors' point of view, a more sophisticated control law for the boundary values, rather than a simple correction proportional to the time-averaged deviation, could possibly provide a massive speedup for large, unsteady multi-passage simulations.

For multi-passage simulations with truly periodic boundaries, in contrast to single passage simulations using the phase lag approach and non-zero IBPA, the circumferential wavenumber $l = 0$ exists in the discrete wavenumber spectrum. We exclude the circumferential zeroth harmonics, disregarding their temporal harmonic index, from the spectral approach to calculate incoming target characteristics. The reason for this is that circumferential zeroth harmonics, i.e. plane waves propagating normal to the boundary surface, lead to temporal fluctuations in instantaneous circumferential averages. This can interfere with the update of mean characteristics to meet given boundary values as long as the temporal Fourier coefficients are not fully converged. Instead, we extrapolate the instantaneous, circumferentially averaged outgoing characteristics

$$\widetilde{c}^{out} = L_{1D}^{out} \left(\widetilde{q} - \overline{q} \right) \tag{19}$$

with $\widetilde{q}$ being the instantaneous area average state in the boundary adjacent cell layer. Thus, $\widetilde{c}^{out}$ also represents plane waves running orthogonally to the boundary. For periodically converged flows, $\widetilde{c}^{out}$ is equivalent to the outward propagating wave reconstructed from all modes $\hat{q}_{(\omega,0)}$. However, this treatment does not depend on temporal Fourier coefficients and can, hence, be carried out locally in time such that it is capable of capturing transient plane wave disturbances at early stages of the simulation.

Finally, we can reconstruct the complete state q for any boundary face. For simulations with truly periodic boundaries q reads

$$q = \overline{q} + \left[R_{1D}^{in} \left(c_{in,f} + \frac{\psi \mathcal{N}}{N} \delta \overline{c^{in}} \right) + R_{1D}^{out} \left(\widetilde{c}^{out} + c'^{out} \right) \right] \tag{20}$$

with $c'^{out} = L_{1D}^{out} \left(q - \widetilde{q} \right)$.

If the phase lag technique is used, $\widetilde{c}^{out}$ must be omitted and q is given by

$$q = \overline{q} + \left[R_{1D}^{in} \left(c_{in,f} + \frac{\psi \mathcal{N}}{N} \delta \overline{c^{in}} \right) + R_{1D}^{out} c^{out} \right] \tag{21}$$

with $c^{out} = L_{1D}^{out}\,(q - \overline{q})$.

3.0 TEST CASES

3.1 Tenth standard configuration

The academic flutter case standard configuration number ten is the first application of the presented NRBC in this paper. It is a well-established numerical flutter experiment for code validation purposes. The two-dimensional flow through a oscillating cascade of modified, cambered NACA0006 airfoils with pitch-to-chord ratio of unity and 45° stagger angle is investigated. For details on the test case and a comprehensive overview of reference results obtained by different authors using a variety of methods see [14].

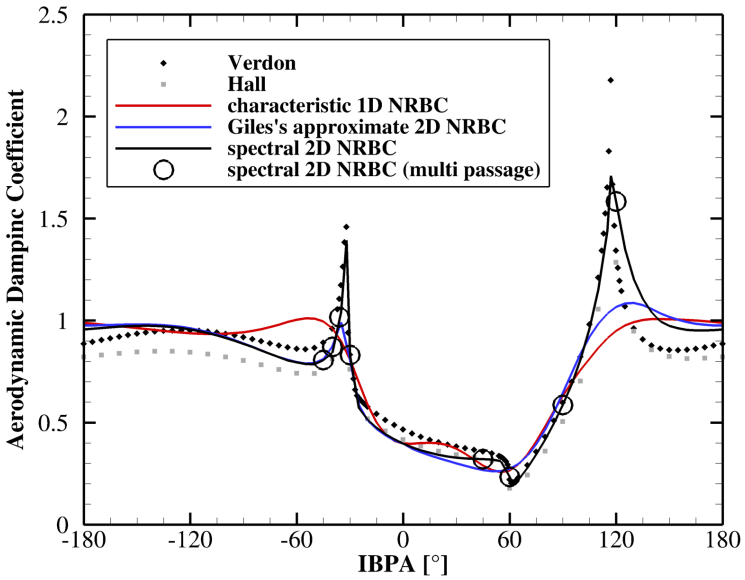

Figure 1: Aerodynamic damping versus inter-blade phase angle.

We consider subsonic flow conditions ($Ma = 0.7$) with a blade pitching motion at reduced frequency $\omega^* = \frac{c\omega}{2U} = 0.5$ with $c/2$ being the half chord length, ω the angular frequency of the pitching motion and U the mean inflow velocity.

These conditions are referred to as cases 3 (σ=0°) and 4 (σ=90°) in the literature. Reference results obtained by Verdon (cf. [20] for the description of his method) and Hall (cf. [21] for his method) are available. This test case is known for being sensitive to possible artificial reflections from the boundaries, in particular in the vicinity of conditions where acoustic resonance occurs.

All simulations in this paper are performed with DLR's in-house CFD code TRACE (cf. [22] and the references therein). We conduct single passage time marching simulations using the phase lag approach for the complete range of possible IBPAs with the presented spectral two-dimensional NRBC as well as with one-dimensional characteristic boundary conditions and Giles's approximate two-dimensional NRBC for comparison. We further perform multi-passage computations with truly periodic boundaries and spectral NRBC for a number of IBPAs, that can be computed using integer blade counts. The flow is assumed to be inviscid and an implicit dual time-stepping BDF2 scheme with 64 time steps per cycle is employed. The pitching motion imposed on the blade has an amplitude of

one degree. The inlet and outlet boundaries are located roughly one chord length away from the leading and trailing edges.

Figure 1 shows that using the spectral two-dimensional NRBC, the predicted aerodynamic damping coefficient $\Xi = \frac{Re(-W_{cyc})}{\pi\alpha^2 c^2 h p_{dyn}}$ agrees well with reference results. Here W_{cyc} represents the aerodynamic work per cycle, α is the pitching angle (radian measure), h the blade span and p_{dyn} the compressible dynamic pressure. The results obtained from the multi-passage simulations agree perfectly with the results from the phase lag computations. This indicates that the special treatment of zeroth spatial harmonics, as described in Section 2.2.2, does not affect the converged solution. In contrast, using the characteristic one-dimensional NRBC yields a qualitatively different damping curve. The distinct peaks at acoustic resonance conditions are not captured correctly. The minimal damping at about 60° is overestimated. Giles's approximate NRBC provides better results than simple characteristic NRBC. They exhibit weak peaks at the correct IBPAs, but in the vicinity of acoustic resonance, the agreement with the references is poor. The accuracy of the approximate NRBCs decreases with increasing absolute value of circumferential wavenumber, i.e. increasing absolute value of the IBPA, because Giles's approach is based on a Taylor series expansion about $l/\omega = 0$. This becomes evident as the peak at $\sigma \approx$-30° is better reflected than the peak at $\sigma \approx 120°$. As at $\sigma = 0°$, the waves leave the domain perpendicularly to the boundary, in this case the predicted damping values of all three NRBCs coincide.

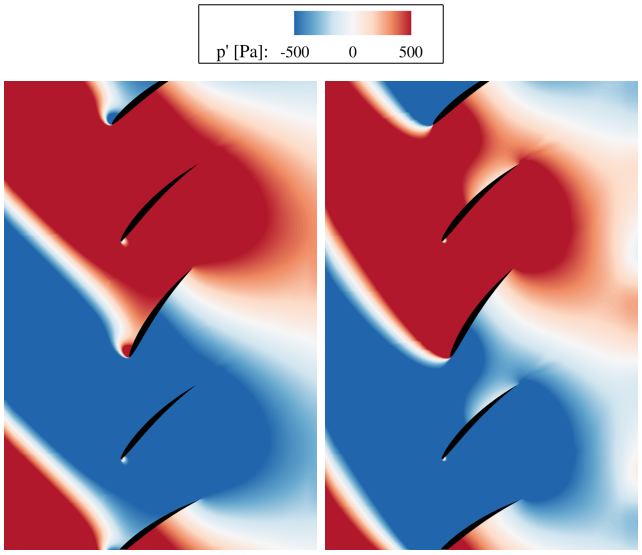

(a) spectral 2D NRBC (b) characteristic 1D NRBC

Figure 2: Snapshot of unsteady pressure fluctuations ($\sigma = 90°$).

The pressure fluctuation arising from the blade pitching motion using the one-dimensional and the spectral boundary condition is depicted in Fig. 2 at the moment of maximum displacement. Note that the actual blade movement is amplified by a factor of ten in this figure for visualisation purposes. We can observe reflections of the one-dimensional NRBC at both boundaries. As, for the given $\sigma = 90°$, the upstream propagating mode at the inflow is cut on, we can expect straight wave fronts. However, when employing one-dimensional boundary conditions, the resulting wave fronts are curved. The reflection of the cut off mode occurring at the outlet with the one-dimensional boundary condition is even more evident.

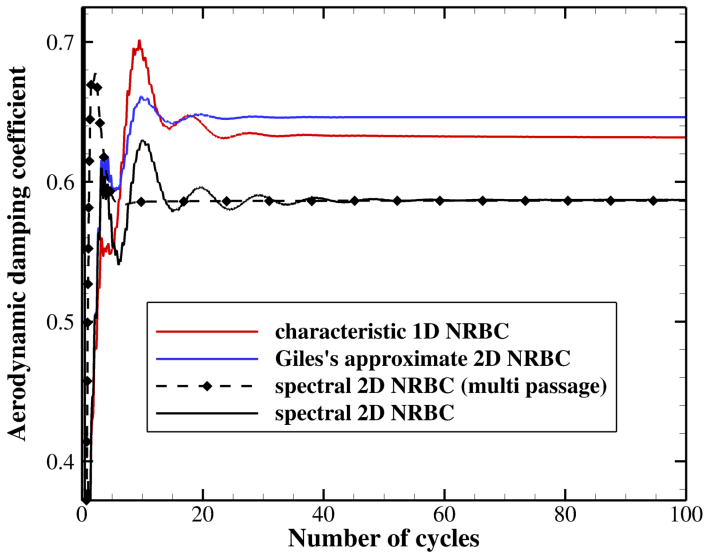

Figure 3: Development of damping coefficient ($\sigma = 90\,°$).

Figure 3 depicts the convergence of the damping coefficient at $\sigma = 90°$. Two things can be observed here: The spectral two-dimensional boundary conditions need more time steps to reach a converged value compared to the one-dimensional and the approximate boundary conditions. However, the multi-passage simulations converge much faster and exhibit no oscillations whereas the curves of phase lag simulations, and in particular the one using spectral NRBC, are less smooth. There are two effects that contribute to this observation. The phase lag approach is per se prone to such oscillations. When additionally the inflow and outflow boundaries depend on slowly converging temporal Fourier coefficients, the harmonic convergence is further lagged. Moreover, it is important that in single passage simulations with non-zero IBPA, the mode with circumferential wave number equal to zero is not part of the expected spectrum. As this mode is not accounted for in the spectral analysis, the aforementioned transient extrapolation of waves that propagate perpendicularly to the boundary is not applicable here.

3.2 DLR's UHBR

The second test case presented in this paper is DLR's Ultra High Bypass Ratio fan rig (cf. [23]). We will focus on the generation and propagation of a discrete tonal noise mode in the following in order to demonstrate the robust applicability of our spectral NRBC implementation to time domain simulations of blade row interactions. In this work, we consider the tonal noise generation under approach conditions. The fan is designed such that, for this operating point, the modes originating from the rotor stator interaction according to the theory of Tyler and Sofrin [24] are cut off at the first wake harmonic. An upstream propagating cut on mode, however, is generated at the second rotor wake harmonic in the downstream stator row. With 22 rotor blades and 38 subsequent vanes, this mode has a nodal diameter of 6. Extensive acoustic studies of the configuration are available [25, 26, 27, 4] which identify this mode to be the primary contribution to tonal noise.

Our computational setup is comparable to the one used in [26] and [4]. The mesh contains about 3.6 million grid points and resolves the acoustic mode of interest with about 40 points per wavelength. From the study of temporal discretisation

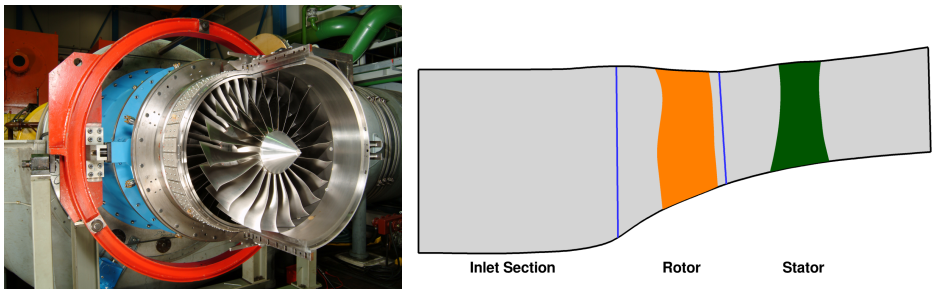

(a) Installation of the UHBR in DLR's test facilities

(b) Computational domain

Figure 4: DLR's Ultra High Bypass Ratio fan.

accuracy in [26], an implicit Crank-Nicolson scheme [28] with 64 time steps per blade interaction cycle is selected as a good compromise between computational costs and numerical accuracy. We conduct multi-passage simulations comprising 180° pitch resulting in 11 to 19 blades per row (denoted in the following figures by suffix "MP") and single passage simulations using the phase lag approach. For comparison, we also repeated the Harmonic Balance computations from [4] with three harmonics resolved in both rows. If not labeled by the suffix "long", all computations are performed using a shorter domain without the inlet section (see Fig. 4b).

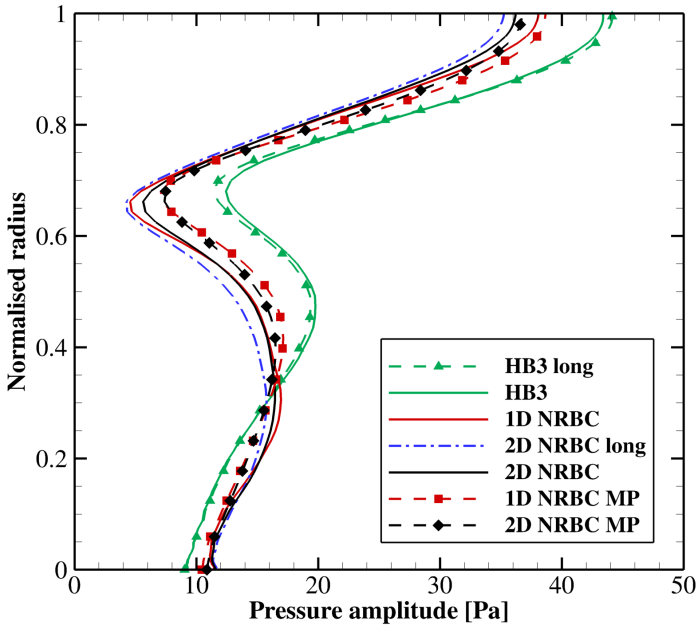

Figure 5: Pressure amplitude of predominant Tyler-Sofrin mode (m=6, ω = 2 BPF) at the rotor-stator interface.

In all computations, the operating point (m^*_{red} = 0.463, Π^* = 0.730) remains constant and matches the conditions of [26]. The sound generation mechanism is captured in very good agreement by all configurations as illustrated by Fig. 5. It plots the pressure amplitude of the relevant Tyler-Sofrin mode against the radial position along the interface between the rotor and the stator domain. The impact

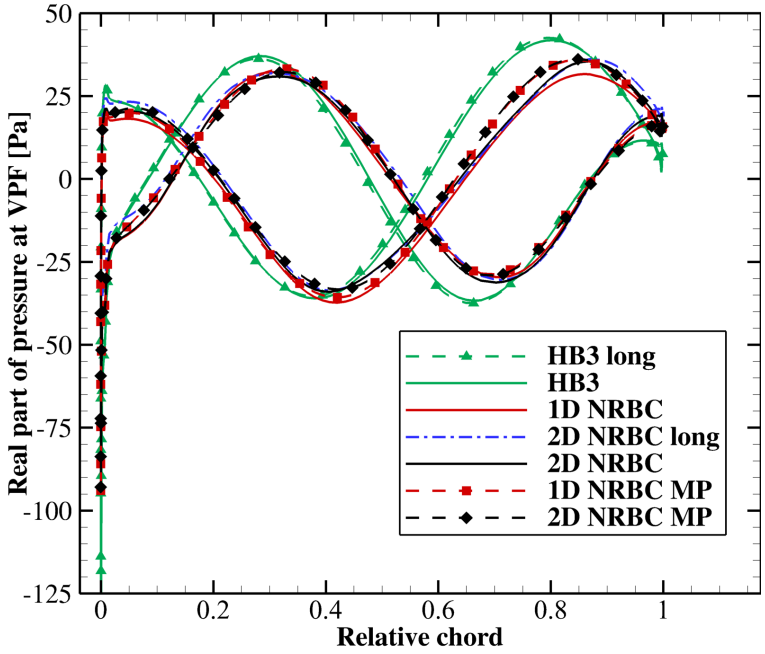

Figure 6: Real part of pressure fluctuations at first vane passing harmonic along the fan blade at 85 % normalised span.

of the boundary condition method and location on the blade row interaction is minor. The solutions of phase lag and multi-passage simulations agree well, but do, in contrast to the results in Section 3.1, not perfectly coincide. The frequency domain solutions correspond to the results in [4]. The predicted pressure amplitudes are 5-10 Pa stronger than in the time domain results. This observation may be explained by the dissipation error in the time domain. The temporal resolution and discretisation scheme was selected with focus on how to efficiently obtain sufficiently accurate results for this numerical study rather than the best possible, but costly accuracy. Yet, we deem the time domain results describe the principal effects of tonal noise generation well enough to demonstrate the applicability of spectral NRBC to the investigation blade row interaction phenomena.

A similar conclusion can be drawn from Fig. 6. It depicts the real part of the temporally Fourier-transformed pressure on the rotor blade at the first vane passing harmonic along a cut at 85% normalised span. Due to the relative motion of the rotor and the stator frame of reference, the upstream propagating mode is mapped to this frequency in the rotor domain (cf. [4]). The fact, that the blade pressure distributions obtained with the long domain and the truncated domain strongly agree, implies that the flow solution is not polluted by spurious reflections from the boundaries. The solutions predicted using characteristic one-dimensional NRBC match as well. This is due to the outgoing mode being highly cut on, i.e. it passes the inflow boundary nearly perpendicularly, shown in Fig. 7. Therefore, one-dimensional NRBC, which assume all perturbations propagate orthogonally to the boundary, provide reasonable results for this configuration. However, the purpose of this test case is to demonstrate that our implementation of spectral NRBC is robust and can be employed for realistic turbomachinery configurations. Nevertheless, Section 3.1 and a previous application of these boundary conditions to the flutter analysis of a transonic low pressure steam turbine blade [29] show the superior reflection properties of the spectral two-dimensional NRBC and why insufficient boundary conditions can deteriorate the flow solution.

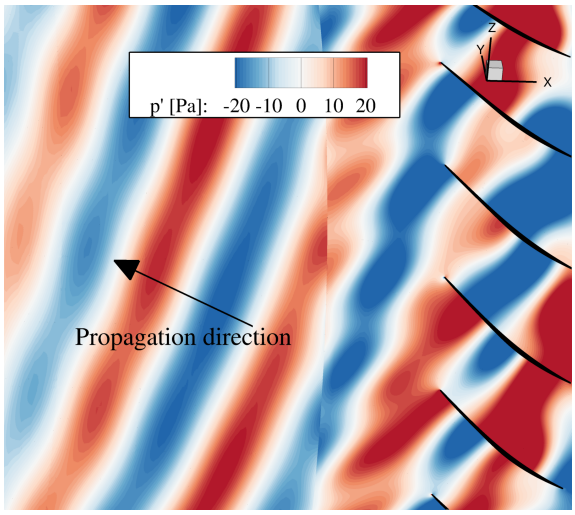

Figure 7: Snapshot of instantaneous pressure fluctuations in the blade-to-blade surface at 50 % normalised radius reconstructed from three harmonics.

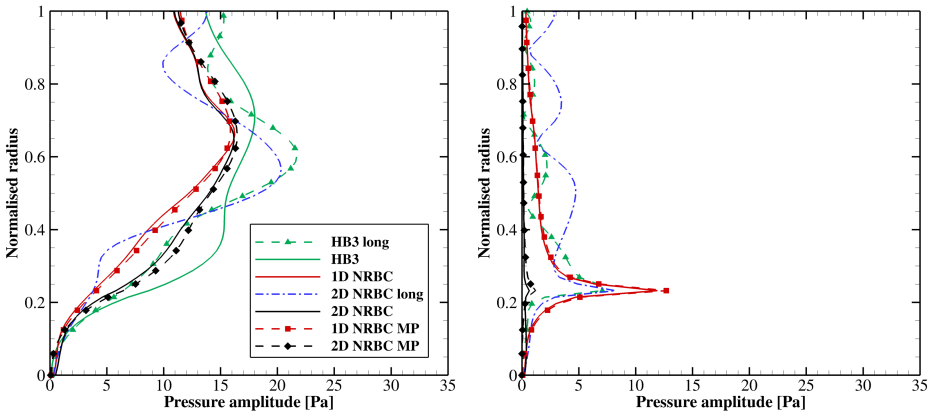

(a) Entire amplitude

(b) Amplitude of downstream propagating wave

Figure 8: Pressure amplitude of predominant Tyler-Sofrin mode (m=6, ω = VPF) at rotor inlet.

Although the solution within the domain is not considerably affected by numerical reflections, we investigate the flow field at the interface between the inlet section and the rotor domain, which is the inflow boundary of all computations using the shorter domain. Figure 8a depicts the radial distribution of the same mode that is inspected at the rotor-stator interface in Fig. 5. The solutions obtained with the full domain reveal that the flow field at this position contains radial modes and, therefore, cannot be considered primarily two-dimensional. Imposing one- or two-dimensional boundary conditions at this position suppresses these modes. Thus, a longer inlet section in front of the analysis plane or three-dimensional boundary conditions are required for a proper aeroacoustic analysis of tonal noise emissions. In this case, however, the truncation of the computational domain is intended to investigate the boundary conditions under more demanding conditions.

However, the plot also exhibits different modal amplitudes depending on the choice of boundary conditions. Figure 8b shows the amplitude of the downstream travelling share of the entire modal amplitude according to the two-dimensional wave

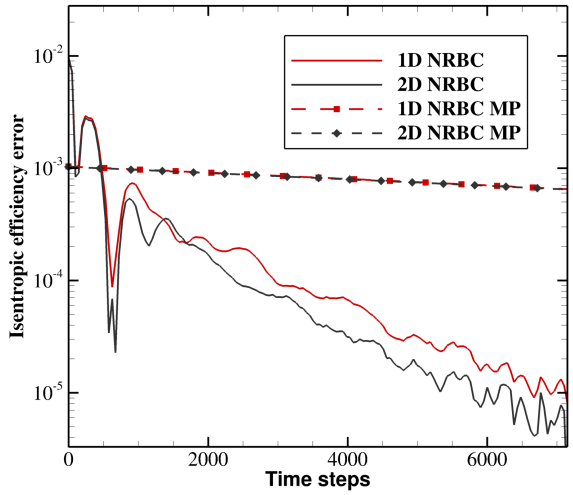

Figure 9: Development of isentropic efficiency error with respect to final value.

decomposition (Eqn. (8)). The strong peak at about 20 % normalised span is an artefact of the decomposition becoming nearly singular under acoustic resonance conditions. But at larger radii, we observe a small amplitude of the incoming wave in the results obtained with one-dimensional boundary conditions. This incoming wave constitutes an artificial reflection. But as its amplitude is small, it has only negligible impact on the interior solution.

Figure 9 plots the development of the deviation of isentropic efficiency from its converged value. The plot confirms that in terms of robustness and convergence speed, the spectral NRBC are similar to the well-established one-dimensional NRBC. Note that for the multi-passage computations, the total number of performed time steps to achieve a comparable level of convergence is 48,640, corresponding to 40 passing cycles of the half wheel segments. The plot is truncated here for clarity. The multi-passage simulations converge much slower than the single passage phase lag simulations. This is due to the fact that the fundamental frequency of the multi passage simulations is the much smaller half wheel passing frequency in comparison to the blade passing frequency in the single passage simulations. Therefore, temporally averaged quantities develop slowly and the incremental update of the mean boundary values must be small as discussed in Section 2.2.

4.0 CONCLUSIONS

We have implemented spectral two-dimensional non-reflecting boundary conditions in DLR's CFD solver for turbomachinery flows TRACE. NRBC of this type are employed in many frequency domain solvers and offer desirable suppression of spurious reflections. However, they are non-local in time and space and, hence, their implementation is considered intricate. We have addressed several aspects that arise when spectral NRBC are used for time domain simulations with dual time-stepping. A formulation based on characteristic variables is helpful because the boundary condition remains stable if incoming characteristics are appropriately relaxed. The distinction which steps of the boundary condition algorithm must be conducted in physical time and which steps in pseudo-time is also vital.

For validation we have applied the spectral boundary conditions to two test cases. Firstly, the flutter analysis of the tenth standard configuration has shown that the spectral NRBC provide improved reflection properties required for the correct prediction of aerodynamic damping. The prediction of the predominant Tyler-Sofrin

mode in DLR's UHBR fan has proved that the presented NRBC can be used for the simulations of blade interaction phenomena in relevant turbomachinery configurations. We have shown that our implementation works for both multi-passage simulations and single passage simulations using the phase lag technique with excellent agreement. Both test cases illustrate that the robustness and convergence properties of the implementation of spectral NRBC presented in this work are comparable to those of a simple, one-dimensional characteristic NRBC. Towards a previous implementation of spectral NRBC in TRACE, this is regarded by the authors as a substantial improvement.

REFERENCES

[1] L He and W Ning. "Efficient approach for analysis of unsteady viscous flows in turbomachines". *AIAA J.*, volume 36, no. 11:pp. 2005–2012, 1998. doi:10.2514/2.328. URL `https://doi.org/10.2514/2.328`.

[2] K. C Hall, J. P Thomas and W. S Clark. "Computation of unsteady nonlinear flows in cascades using a harmonic balance technique". *AIAA J.*, volume 40, no. 5:pp. 879–886, 2002. doi:10.2514/2.1754. URL `https://doi.org/10.2514/2.1754`.

[3] M. S McMullen. *The Application of Non-Linear Frequency Domain Methods to the Euler and Navier-Stokes Equations*. Phd thesis, Stanford University, 2003.

[4] C Frey, G Ashcroft and H.-P Kersken. "Simulations of unsteady blade row interactions using linear and non-linear frequency domain methods". In "ASME Turbo Expo 2015: Turbine Technical Conference and Exposition", 56642, 2015. doi:10.1115/gt2015-43453.

[5] H.-P Kersken, G Ashcroft, C Frey et al. "Nonreflecting boundary conditions for aeroelastic analysis in time and frequency domain 3D RANS solvers". In "Proceedings of ASME Turbo Expo 2014", 2014.

[6] M. D Montgomery and J. M Verdon. "A three-dimensional linearized unsteady euler analysis for turbomachinery blade rows". Technical Report NASA CR-4770, United Technologies Research Center, East Hartford, Connecticut, USA, 1997.

[7] P Moinier, M. B Giles and J Coupland. "Three-dimensional nonreflecting boundary conditions for swirling flow in turbomachinery". *J. Propul. Power*, volume 23, no. 5:pp. 981–986, 2007.

[8] P. J Petrie-Repar. "Three-dimensional non-reflecting boundary condition for linearized flow solvers". In "Proceedings of the ASME Turbo Expo 2010: Power for Land, Sea, and Air", pp. 1247–1252. American Society of Mechanical Engineers, 2010.

[9] M. B Giles. "Non-reflecting boundary conditions for the Euler equations". Technical report, MIT Dept. of Aero. and Astr., 1988. CFDL Report 88-1.

[10] J Chassaing and G Gerolymos. "Time-domain implementation of non-reflecting boundary-conditions for the nonlinear euler equations". *Applied mathematical modelling*, volume 31, no. 10:pp. 2172–2188, 2007.

[11] D Schlüss, C Frey and G Ashcroft. "Consistent non-reflecting boundary conditions for both steady and unsteady flow simulations in turbomachinery applictations". In M Papadrakakis, V Papadopoulos, G Stefanou et al. (editors), "VII European Congress on Computational Methods in Applied Sciences and Engineering (ECCOMAS Congress 2016)", 2016.

[12] J Goodrich and T Hagstrom. "Accurate algorithms and radiation boundary conditions for linearized euler equations". In "Aeroacoustics Conference", p. 1660. 1996.

[13] C Frey, G Ashcroft, H.-P Kersken et al. "A harmonic balance technique for multistage turbomachinery applications". In "ASME Turbo Expo 2014: Turbine Technical Conference and Exposi-

tion", p. V02BT39A005. 45615, 2014. doi:10.1115/gt2014-25230. URL http://dx.doi.org/10.1115/GT2014-25230.

[14] T. H Fransson and J. M Verdon. "Updated report on Standard Configurations for the Determination of unsteady Flow Through Vibrating Axial-flow Turbomachine-Cascades". Technical Report TRITA/KRV/92.009, KTH, Stockholm, 1992.

[15] C Frey and H.-P Kersken. "On the regularisation of non-reflecting boundary conditions near acoustic resonance". In "ECCOMAS Congress 2016 VII European Congress on Computational Methods in Applied Sciences and Engineering, Crete Island, Greece", 2016.

[16] L He. "An euler solution for unsteady flows around oscillating blades". *Journal of Turbomachinery-transactions of the Asme*, volume 112, no. 4:pp. 714–722, 1990. doi:10.1115/1.2927714.

[17] L He. "Method of simulating unsteady turbomachinery flows with multiple perturbations". *AIAA J.*, volume 30, no. 11:pp. 2730–2735, 1992. doi:10.2514/3.11291.

[18] M Giles. "UNSFLO: A numerical method for the calculation of unsteady flow in turobmachinery". Technical report, Gas Turbine Laboratory Report GTL 205, MIT Dept. of Aero. and Astro., 1991.

[19] N. A Cumpsty and J. H Horlock. "Averaging nonuniform flow for a purpose". *J. Turbomach.*, volume 128, no. 1:pp. 120–129, 2006.

[20] J. M Verdon and W. J Usab. *Application of a linearized unsteady aerodynamic analysis to standard cascade configurations*. National Aeronautics and Space Administration, 1986.

[21] K HALL and W CLARK. "Prediction of unsteady aerodynamic loads in cascades using the linearized euler equations on deforming grids". In "27th Joint Propulsion Conference", AIAA-3378, 1991.

[22] K Becker, K Heitkamp and E Kügeler. "Recent progress in a hybrid-grid cfd solver for turbomachinery flows". In "Proceedings Fifth European Conference on Computational Fluid Dynamics ECCOMAS CFD 2010", Lisbon, Portugal, 2010.

[23] B Kaplan, E Nicke and C Voss. "Design of a highly efficient low-noise fan for ultra-high bypass engines". 2006. ASME Paper No. GT2006-90363.

[24] J. M Tyler and T. G Sofrin. "Axial flow compressor noise studies". *Transactions of the Society of Automotive Engineers*, volume 70:pp. 309–332, 1962.

[25] C Weckmüller, S Guerin and G Ashcroft. "CFD/CAA coupling applied to the DLR UHBR-fan: Comparison to experimental data". In "Proceedings of the *15th AIAA/CEAS Aeroacoustics Conference*, Miami, USA", 2009.

[26] G Ashcroft, C Frey, K Heitkamp et al. "Advanced numerical methods for the prediction of tonal noise in turbomachinery - part i: Implicit runge-kutta schemes". *J. Turbomach.*, volume 136, no. 2:pp. 021002–021002–9, 2013. ISSN 0889-504X. doi:10.1115/1.4023904. URL http://dx.doi.org/10.1115/1.4023904.

[27] C Frey, G Ashcroft, H.-P Kersken et al. "Advanced numerical methods for the prediction of tonal noise in turbomachinery, Part II: Time-linearized methods". *ASME Paper No. GT2012-69418*, 2012.

[28] J Crank and P Nicolson. "A practical method for numerical evaluation of solutions of partial differential equations of the heat-conduction type". In "Proceedings of the Cambridge Philosophical Society", pp. 50–67. 43, 1947.

[29] D Schlüss and C Frey. "Time domain flutter simulations of a steam turbine stage using sptectral 2d non-reflecting boundary conditions". In "15th International Symposium on Unsteady Aerodynamics, Aeroacoustics & Aeroelasticity of Turbomachines (ISUAAAT15)", 2018.